Low frequency (LF) radio sounding for ionospheric remote sensing and earthquake prediction (case study a few earthquakes in North-West Iran)

Mohsen Safari[1], Alireza Mahmoudian*[2], Mehdi Rezapour[3]

1. MSc Graduate, Department of Seismology, Institute of Geophysics, University of Tehran, Tehran, Iran.
2. Assistant Professor, Department of Space Physics, Institute of Geophysics, University of Tehran, Tehran, Iran.
3. Professor, Department of Seismology, Institute of Geophysics, University of Tehran, Tehran, Iran.
*Corresponding Author E-mail: a.mahmoudian@ut.ac.ir

1. Abstract

This paper presents the first low frequency (LF) radio sounding in Iran for earthquake prediction and ionospheric remote sensing purposes. Two LF signal transmitted from Turkey (162 kHz) and Tajikistan (252 kHz) are recorded in Tehran. The recorded data in 2019 is studied in detail. The diurnal variation of the LF signal is averaged over one month period to remove temporal variations as a result of background ionospheric irregularities as well as pre-seismic anomalies. The capability of the International Reference Ionosphere (IRI) model in explanation of the time evolution of the received signal is examined. The morning and evening termination time manifested from amplitude of the received LF signal is compared against the variation of electron density obtained along the transmitter-receiver great circle path. It has been shown that simple comparison of the averaged electron density along the signal propagation path from the transmitter to the receiver can be used to estimate the electron density during sunset and sunrise. A comprehensive method to advance the IRI estimation of the current state of the ionosphere is proposed. The LF signal anomalies associated with 4 earthquake (EQ) events in the vicinity of the propagated LF signals at 162 kHz from Turkey to Tehran is investigated. The anomalous behavior of the LF signal within +/-15 days of the EQ is studied. Daytime variation as well as sunrise and sunset offset in days approaching each event is explored as a possible indicator of pre-seismic activity. The characterization of the LF radio signal and the possibility of the earthquake prediction within Iran plateau are discussed.

Keywords: low frequency, radio sounding, remote sensing, EQ precursors

2. Introduction

To mitigate the catastrophic impacts of strong earthquakes, scientists have implemented new techniques to achieve short term earthquake prediction. One of the well-known approaches for earthquake prediction within a few weeks to a few days leading to the event is using the radio sounding at different frequency bands to detect seismo-ionospheric anomalies in the propagation of radio signal (Pulinets and Ouzounov, 2011; Hayakawa, 2016; Ouzounov et al., 2016). The lithosphere-atmosphere-ionosphere coupling (LAIC) accompanied by radon emanation before an EQ leads to a change in atmospheric conductivity due to enhanced ionization near the surface (Pulinets and Boyarchuk, 2004; Pulinets and Ouzounov, 2011). Ion hydration through absorption of water vapor present in the air leads to latent heat release and reduced air conductivity near the EQ epicenter. As the ion hydration and absorption of air-water vapor proceed, the ions become larger and less mobile. This process leads to latent heat release and reduced air conductivity near the EQ epicenter. Atmospheric gravity wave can form as a result of temperature or pressure gradient (Yang et al., 2019, Yang and Hayakawa, 2020; Kundu et al., 2022; Ghosh et al., 2022). As the ion aging process advances, heavy aerosol particles start to form. This has been proposed as the chain of processes leading to ionospheric perturbation through reduced electric potential between the earth and the ionosphere (Pulinets and Boyarchuk 2005; Pulinets and Ouzounov 2011; Sorokin et al. 2015; Hayakawa et al. 2021). Earthquake precursors from the space to the ground have been investigated over the years (Picozza et al., 2021; Conti et al., 2021). This has been proposed as the main consequence leading to ionospheric perturbation through reduced electric potential between the earth and the ionosphere and results in radiowave distruption in the LF and VLF bands (Molchanov et al.,

2004; Pulinets and Boyarchuk, 2004; Pulinets and Ouzounov 2011; Sorokin et al., 2015; Hayakawa et al., 2021).

One of the early works of earthquake prediction using radio-waves in the very low frequency (VLF) band was reported by Hayakawa et al. (1996) associated with the Kobe earthquake on January 17, 1995. A notable shift in the termination time including morning termination time to early hours and evening termination time to later hours were observed. Hayakawa et al. (1996) and Molchanov et al. (1998) proposed a change in the propagation mode due to interference introduced as a result of electromagnetic phenomena in the LAIC system. The previous studies have revealed a positive correlation of VLF anomalies with EQ magnitude and negative relation with EQ depth. Several other parameters could affect the order of such correlation including the geolocation of earthquake and related local meteorological aspects involved in the LAIC process as well as the distance and frequency of the radio transmitter and receiver. Therefore, a comprehensive study over many years is required before a substantial-conclusion can be made on this subject. Another detailed study of VLF and lower LF band radio-waves utilizing superimposed epoch analysis and standard deviation (σ) with +/-15 of the EQ was presented by Hayakawa et al. (2010). The nighttime fluctuation shows a convincing enhancement 12 days before the EQ only for stronger EQs. Nighttime average amplitude showed a depletion effect with σ value of below -2 associated with strong earthquakes of 5 to 7 in magnitude, about ~12 days before the EQ. What can be noted from the results presented by Hayakawa et al. (2010) is that nighttime average amplitude and nighttime fluctuation illustrate the minimum deviation close to the EQ day. More recent studies on subionospheric VLF perturbations observed at low latitude associated with earthquake have been reported by Kumar et al. (2014, 2021). A newly developed Doppler shift radar observation using Doppler shifts of short-distance subionospheric signal (lower LF band ~40 kHz) has shown to be a promising tool for the diagnostics of seismo-ionospheric (Asai et al., 2011).

Low frequency (LF) is in the range of 30–300 kHz, with wavelengths range from 10–1 km, respectively. The LF radio waves exhibit low signal attenuation, making them suitable for long-distance communications. In Europe and areas of Northern Africa and Asia, part of the LF spectrum is used for AM broadcasting as the "longwave" band. In the western hemisphere, its main use is for aircraft beacon, navigation, information, and weather systems. A number of time signal broadcasts also use this band. Low frequency waves can also occasionally travel long distances by reflecting from the ionosphere (the actual mechanism is one of refraction), although this method, called skywave, is not as common as at higher frequencies. Reflection occurs at the ionospheric E layer or F layers. Skywave signals can be detected at distances exceeding 300 km from the transmitting antenna. This is the main basis of the proposed technique in this paper. As a result of skywave LF propagation, the received LF wave amplitude should show temporal evolution corresponding to the time evolution of ionospheric electron density over the propagation path. Therefore, such a technique is employed and introduced in this paper through calculation signal morning and evening termination time as a consequence of electron density increase and decrease during sunrise and sunset along the propagation path. Then careful comparison with the averaged electron density using IRI model along the transmitter-receiver great circle path (TRGCP) with the measurements is proposed to improve IRI empirical model using such approach.

While the VLF radio sounding has been studied extensively in recent years as a powerful ionospheric remote sensing tool (Cohen et al., 2010; 2018; Gross and Cohen, 2021; Richardson and Cohen, 2021; Mahmoudian et al., 2021), the upper-band LF sounding has been overlooked. The main contribution of the pre-seismic activities and coupling to the lower ionosphere, will modulate the lower altitude of the ionosphere. Such variation will affect the reflection altitude associated with VLF/LF signal and will be manifested in amplitude and phase of the signal. The main objective of the present work is to investigate the reliability of LF sounding in Iran, the possibility of improving empirical ionospheric models such as International Reference Ionosphere (IRI) (Rawer, 1978; Bilitza et al., 2017; Bilitza,

2018), and characterizing the LF signal anomalies associated with pre-earthquake processes. Such an effect can be investigated using the IRI model and be implemented as a practical tool to improve such models. There is convincing evidence that the lower ionosphere is definitely perturbed mainly prior to an EQ. The first part of this study is dedicated to the annual variation of the LF signal that sounded over Iran. The characteristics of the signal are determined and compared with ionospheric plasma variation obtained through the IRI and along with the propagation of the radio signal. The capability of the proposed techniques in improving the IRI forecasting is examined. In the last part, one EQ along the two LF signal transmitted from Turkey and received in Tehran is studied within 15 days prior to and after the event. The main signal characteristics such as morning and evening termination time and daytime variation according to the received signal amplitude are explored. The unique signal features associated with the event and the possibility of prediction are discussed.

3. Methodology and data processing

The Tehran VLF-LF station was set up to receive 5 low frequency (LF) signal throughout the year2019. To plot the amplitude of LF signal versus time, the collected LF data in 1-minute time resolution recorded based on local time in the text format are used (Figures 2 and 3). To obtain monthly averaged data, we averaged the daily data on 1-minute basis using the Matlab software (Figure 4a, b and 5a, b).

The electron density along with TRGCP corresponding to the two studied paths is derived from the IRI model. The electron density altitude profile in the range of 80- 140 km is studied in order to validate the diurnal time variation of the sounded VLF signals. The electron density variation at the selected station over the propagation path of the VLF signal is determined using the IRI model. It should be noted that the first point in each figure denotes the plasma density at the transmitter location and the last point corresponds to the receiver location in Tehran. The corresponding figures 4c, d and 5c, d have a one-hour time resolution. This approach is critical to verify the validity of the recorded data.

There are 4 time periods that are the main focus of this study. The decay time, the minimum amplitude time period and recovery time which are associated with sunrise and sunset termination time. The termination time associated with morning and afternoon is determined using the amplitude change by a factor of 90 percent with respect to the minimum or maximum amplitude, respectively. This method is implemented to obtain Figure 8.

4. Observational results and analysis

As mentioned above, the International Reference Ionosphere (IRI) model is used in this paper to analyze the observational data. The IRI model is a widely used tool to predict the behavior of the Earth's ionosphere. It provides values for various parameters, such as electron density, temperature, and ion composition. This model is updated regularly by the IRI Working Group and is available as a software package containing FORTRAN subroutines. The major data sources are implemented in the IRI model including the worldwide network of ionosondes, the powerful incoherent scatter radars (Jicamarca, Arecibo, Millstone Hill, Malvern, St. Santin), the ISIS and Alouette topside sounders, and in situ instruments flown on many satellites and rockets. Electron density, electron temperature, ion temperature, ion composition (O^+, H^+, He^+, N^+, NO^+, O_2^+, Cluster ions), equatorial vertical ion drift, vertical ionospheric electron content F1 probability, spread-F probability, auroral boundaries, effects of ionospheric storms on F and E peak densities are incorporated in this empirical model."

The experimental observations at the Tehran station includes the received data from 5 VLF transmitters as well as 5 LF transmitters around Iran are performed. The 5 VLF transmitters include 16.2 kHz (KAH, India), 18.2 kHz (VTX, India), 20.5 kHz (RJH, Belarus), 22.2 kHz (JJI, Japan), 26.7 kHz (TBB, Turkey). The 5 LF received signal at the Tehran station were transmitted at 162 kHz

(TRT4, Turkey), 171 kHz (RCH, Russia), 180 kHz (TRT40, Turkey), 252 kHz (TAJ, Tajikistan), 279 kHz (TUR, Turkmenistan). The location of the LF and VLF transmitters with respect to the Tehran receiver is shown in Figure 1 in order to determine the propagation path of the radio signal. To eliminate artificial effect of the sounded LF signal such as short term ionospheric effects as well as pre-seismic anomalies coupled to ionosphere through LAIC process, an averaged signal over entire month with one minute time resolution are calculated. Then, 5 points with approximately equal distances based on the distance between the transmitter and receiver along the TRGCP are selected (shown in Figure 1c). The electron density along with TRGCP corresponding to the two studied paths is derived from the IRI model. The electron density altitude profile in the range of 80-140 km is studied in order to validate the diurnal time variation of the sounded LF signals. The electron density variation at the selected station over the propagation path of the VLF signal is determined using the IRI model. Figures 2 and 3 show the averaged electron density in the altitude range of 80 to 140 km corresponding to the Tajikistan and Turkey transmitters, respectively.
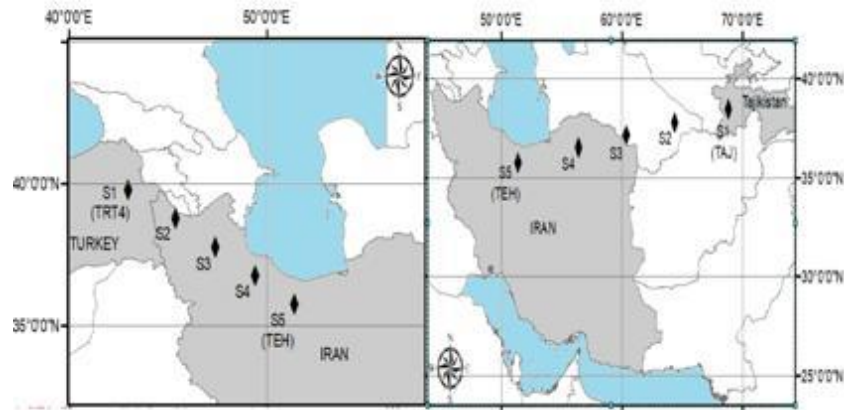
(a)

(b)
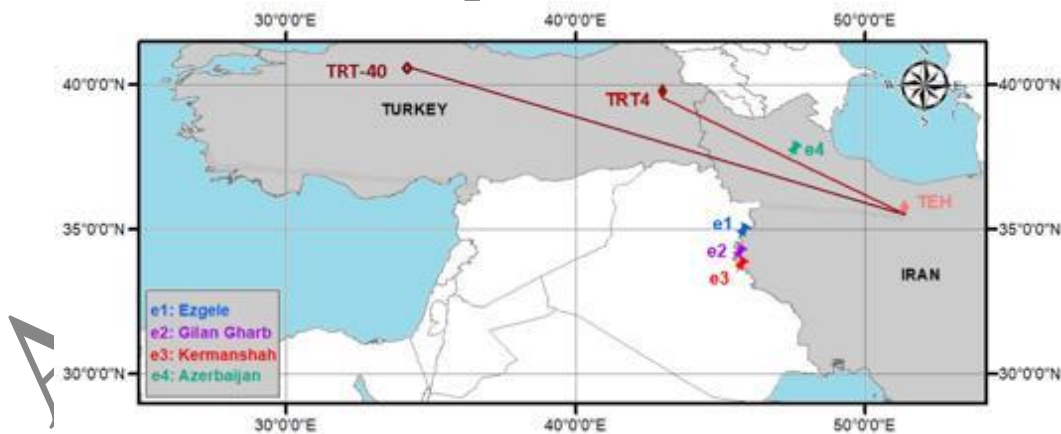
(c)

Figure 1. a) Geographical location of the LF transmitters around Iran with the respect to the receiver position in Iran. b) The geographical location of the two LF transmitters in Turkey and the receiver position in Iran. The locations of 4 selected earthquakes including East Azerbaijan, Ezgeleh, Gilangharb, and Kermanshah in 2019 are shown. c) The propagation path of LF wave with frequency 162 KHZ from Turkey and LF wave with frequency 252 KHZ from Tajikistan to Tehran receiver and the places used in calculating the electron density from the IRI model

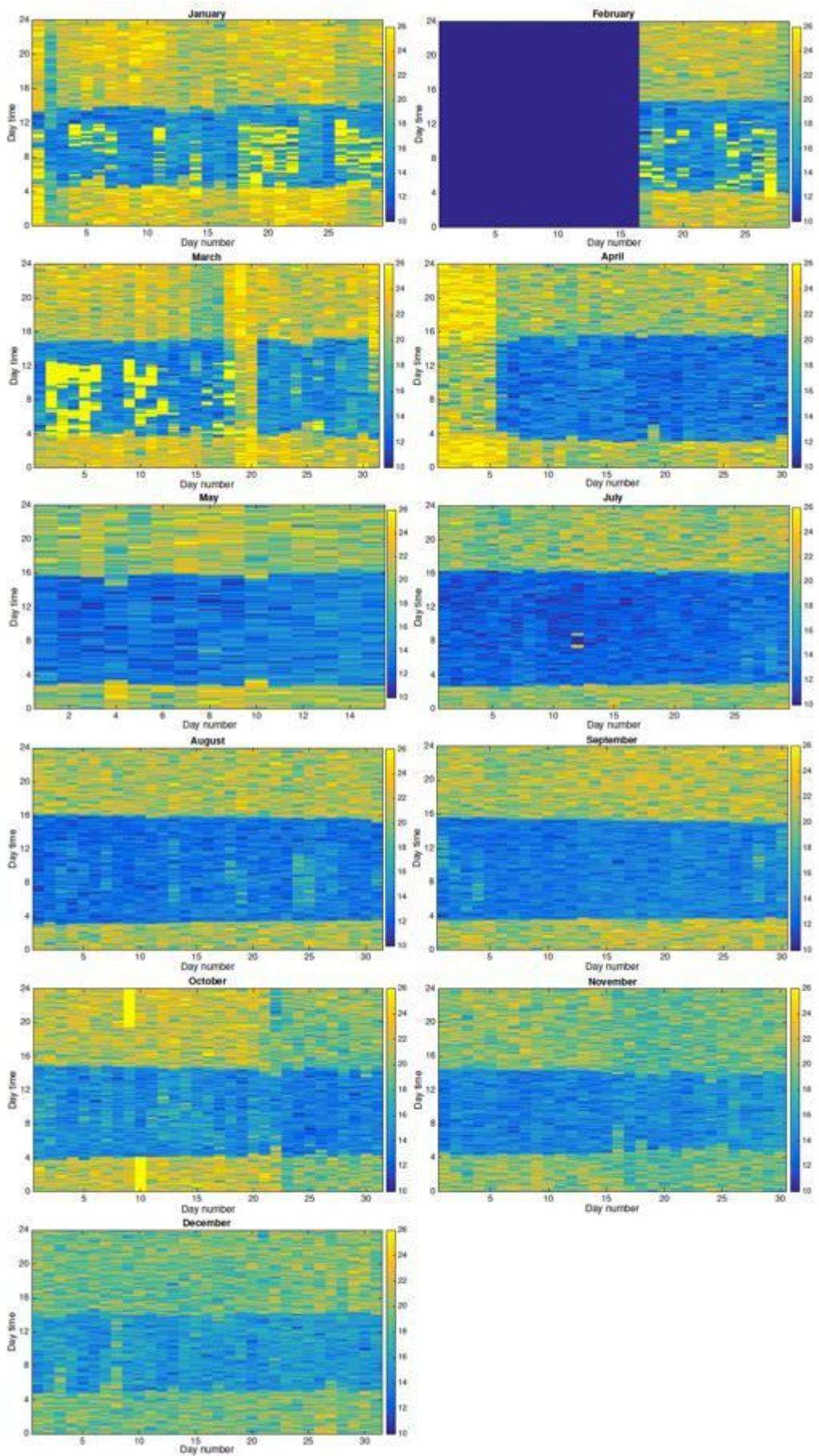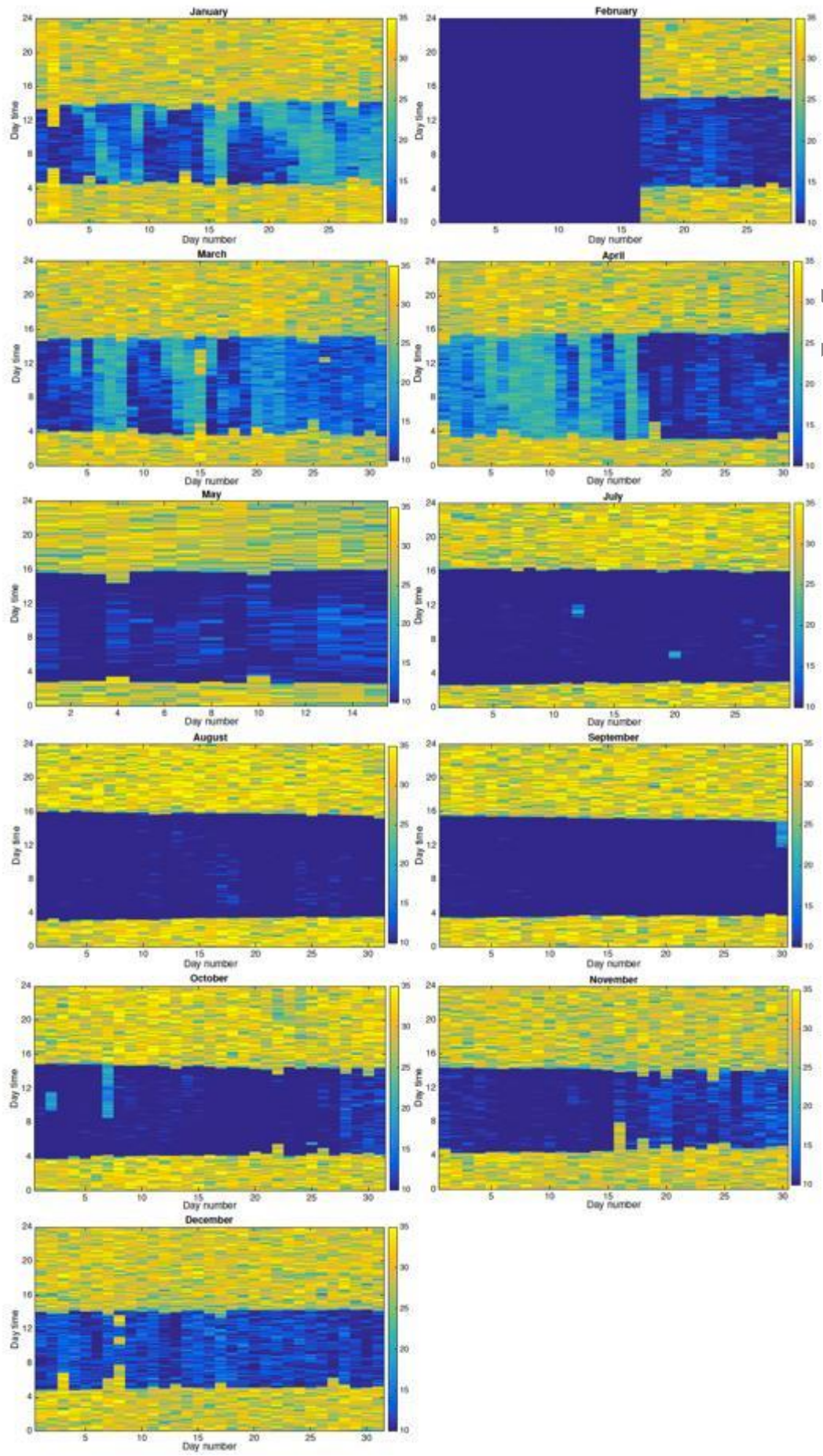Figure 2. Daily and hourly variation of 252 kHz signal in 2019

Figure 3. Daily and hourly variation of 162 kHz signal in 2019

Table 1: Information regarding the studied earthquake events in this paper.

EQ	Date (time in UT)	Coordinates	Depth (km)	M
Ezgeleh	2019-05-11 (18:18:17)	(34.87◦ N, 45.95◦E)	8	5.1
Gilan Gharb	2019–01-06 (13:41:59)	(34.15◦ N, 45.65◦ E)	10.9	5.9
Kermanshah	2019–04-1 (10:28:59)	(33.72◦ N, 45.7◦ E)	16	5.1
Azerbaijan	2019-11-7 (11:43)	(37.71◦ N, 47.52◦ E)	9	6

The Figures 2 and 3 show the daily and variation of the LF signals at 252 and 162 kHz presented in the paper with 1-minute time resolution. It should be noted that the LF data for June 2019 is missing as a result of technical issues. The new figures show that the upper band LF signal is very sensitive to morning and evening termination time. Moreover, the LF data was only recorded for 15 days in February 2019. The general pattern of the signal throughout each month reveals that the averaging of the signal is a good approach to investigate the validity of the signal and prove the remote sensing concept introduced in this paper. It should be noted that, we used the termination time as an indicator of ionospheric morning build up and afternoon decay process. Such timing has been proved to have unresolved chemistry and physics which is being investigated in recent solar eclipse events. Therefore, development and implementation of new techniques such as upper LF radio sounding which is more sensitive to morning and evening termination time can results in improving empirical models such as IRI.

The 252 kHz LF signal transmitted by a radio station in Tajikistan during 2019 was recorded in Tehran station. A close comparison of detected LF signal and its associated behavior in each month is shown in Figure 4a and b. According to this figure, the averaged amplitude of the radio signal in the entire month is used to examine the diurnal variation of the signal. It should be noted that July data is missing due to technical issues. The first three months (January-March) of TAJ (252 kHz) radio signal show an average of 4 dB decrease in signal strength after the sunrise. The start time of initial suppression in signal amplitude between 4:00-5:00 UT follows by a slow increase between 10:00-12:00 UT. The signal shows a sharp decrease subsequent to the previously mentioned behavior. This suppression lasts for about two hours, then the signal recovers to the initial amplitude after the sunset at 14:00 UT, 14:30 UT, and 15:00 UT, corresponding to January, February, and March, respectively. Such an effect could be attributed to additional hob (ionosphere-earth reflection path) as a result of plasma density modulation by induced gravity waves. Such an effect could lead to a strong suppression of radio signals. The associated signals for April (4) and May (5) in Figure 4a show a decrease of ~7 dB in signal strength starting at 3:00 and 2:30, respectively. The rise time occurs at 15:00 UT and 15:30 UT, respectively. The second half of 2019 (July-December) is represented in Figure 4b. The signal amplitude shows a strong correlation with sunrise and sunset time over the propagation path. The duration of signal suppression is ~(5:00-14:00 UT), (4:20-14:20 UT), (4:00-14:30 UT), (3:30-15:20 UT), (3:20-15:45 UT), and (2:40-16:20 UT), respectively, for July-December. There are other general features observed in these figures such as: 1) In the time frame of months 1, 2, and 3 (winter) in the time frame of 3.5 to 14.5 hours, a wave with a large amplitude becomes sinusoidal and the amplitude decreases stepwise.2) In the first 6 months of the year (winter-spring), the time period of decreasing the range increases until it returns to its original state, but in the second 4 months (summer and autumn), this period decreases again. 3) In the first 6 months of the year, the moment of the decline (increase) of the range has a decreasing (increasing) trend and in the second 6 months it has an increasing (decrease) trend.

A close comparison of the normalized accumulated electron density along the propagation path of the radio signal is obtained using the IRI model (shown in Figures 2c, d). The measured signal shows a good agreement in terms of rising and fall time (termination time period). Specifically, the fall in signal strength associated with sunrise as well as the rise in signal strength due to a decrease in electron density at sunset shows an expanding time period from January through June in Figure 4c. An opposite trend with shrinking the time period between sun-rise and -set time from August to December is seen in Figure 4d that confirms the observed behavior in the observed LF radio signal. While the general pattern described above matches well with the observations, an unexpected secondary fall in signal strength between January and March remains an open question. The amplitude of the observed signal also shows a good correlation with maximum electron density predicted by the IRI model, which denotes an increase in the number of reflection paths.
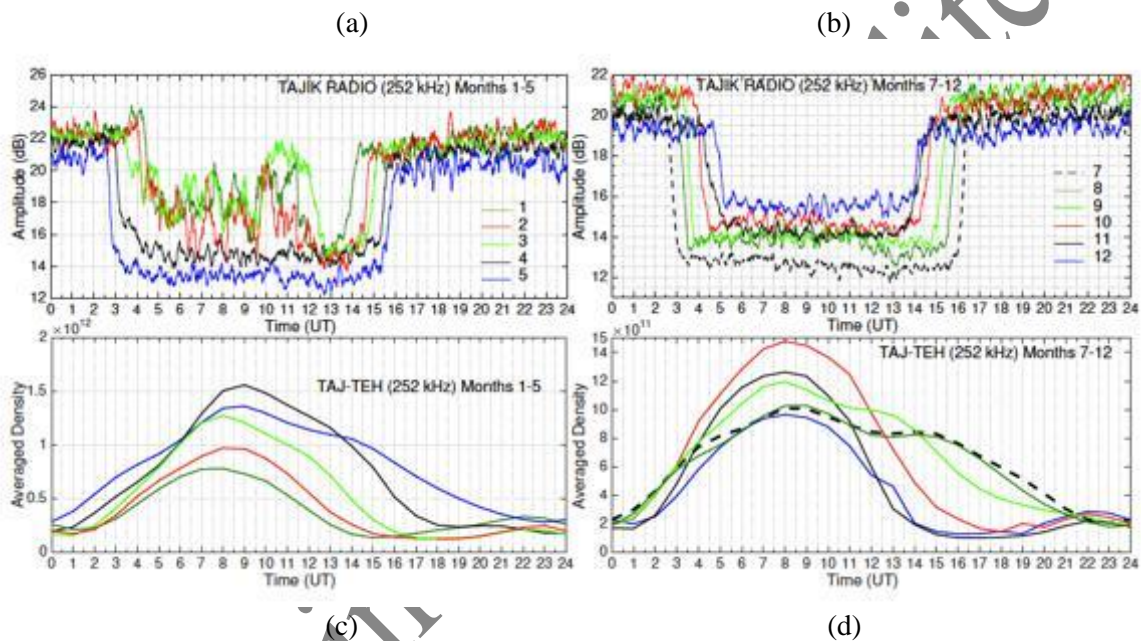
(a)   (b)

(c)   (d)

Figure 4. a, b) Monthly variation of LF radio sounding in Tajikestan-Tehran path at 252 kHz (top panels). c, d) The ionospheric density averaged along the propagation path using the IRI model associated with each month. The panels c and d show the averaged electron density corresponding to panels a and b, respectively.

(a)   (b)
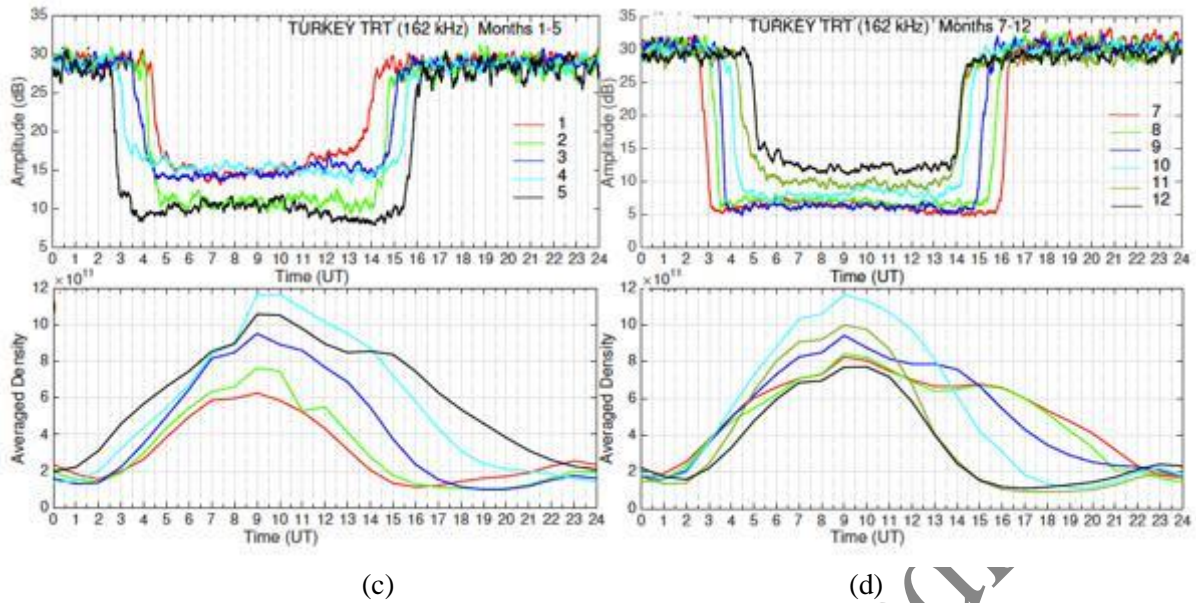
(c)   (d)

Figure 5. Similar to Figure 2 for Turkey-Tehran path at 162 kHz.

The data presented in Figure 5a, b show the diurnal variation of Turkey LF (162 kHz) signal through the year of 2019. It should be noted that each curve associated with each month of the year is obtained using the averaged signal over the entire month. The overall shape and characteristics of the observed signal show consistency throughout the entire year that includes a sharp suppression and a recovery period. There are other features observed in the data that will be listed here: 1) In the first 6 months of the year (winter-spring), the time interval from the reduction of the range until returning to its initial state increases, but in the second 6 months (summer-autumn), this interval decreases again. 2) The difference between the starting range and the ending range is zero except for the 10th and 11th months when this difference reaches 1 to 2 units. 3) In the first 6 months of the year, there is a decreasing trend at the moment of the decline of the range, and an increasing trend in the second 6 months. 4) In the first 6 months of the year, the moment when the range starts to increase has an increasing trend, and in the second 6 months, it has a decreasing trend, but in the 11th and 12th months (autumn-winter), these times are a little unusual and increase.

The fall and rise time of the radio signal over the straight path in the longitudinal direction between Turkey and Tehran shows a good agreement with the rise and fall period of electron density predicted by the IRI model. The averaged electron density along the signal propagation path is shown in Figure 5c and d corresponding to 11 months of the year. The presented data is obtained for the 15th of each month. The duration of suppression (signature of daytime in the LF signal) from January through May increases from 9:30 hours to 13 hours. The electron density data matched well the observational results. From July to December, the duration of the signal suppression period is reduced from 13:40 to 9:20 hours. The termination time obtained from the measurements and IRI calculation are consistent. The relative amplitude of the observed signal and maximum electron density is in agreement to some extent. This could be mainly due to a slight difference in the propagation path as well as a small number of points between the transmitter and receiver considered in this research. Summary of the electron density obtained from the IRI model associated with the morning termination time (T_M) and the evening termination time (T_E) in the Tajik-TEH and TRT4-TEH paths is provided in Table 1. According to this Table, the electron density value including the monthly variation shows a reasonable agreement with the variation of T_M and T_E. As an example, the close variation of T_M for Jan-March in Tajik-TEH path is reflected in the electron density values of $\sim 5*10^{11}$ m^{-3}. It should be noted a better estimation of averaged electron density along the propagation path and associated with T_M and T_E requires more number of points to be considered.

Table 1: Summary of the electron density obtained from the IRI model associated with the morning termination time (T_M) and the evening termination time (T_E) in the Tajik-TEH and TRT4-TEH paths.

	Months	Jan	Feb	Mar	April	May	Jul	Aug	Sep	Oct	Nov	Dec
Tajik	$n_e \times 10^{11} m^{-3}$ sunrise	5	5	5.2	5.2	6	5	5.8	6.4	9.17	8	7
	$n_e \times 10^{11} m^{-3}$ sunset	1.8	2	3	6	8	7.7	7.5	6.8	3.2	1.8	1.8
TRT4	$n_e \times 10^{11} m^{-3}$ sunrise	3.2	3.2	3.2	3.3	4.2	3.6	3.6	4.5	5.4	5.4	4.7
	$n_e \times 10^{11} m^{-3}$ sunset	2	2	3.8	6	7.4	6.4	6.4	6	5	2.2	2.2

5. Earthquake prediction using LF radio sounding

Four earthquakes that occurred on the western border of Iran, and close to the Turkey-Tehran propagation path are studied using LF radio sounding in this paper. The first earthquake studied in this section occurred on 2019-11-07 near East Azerbaijan (AZ) province in the north-west of Iran (37.71 N, 47.52 E) with a magnitude of 6. The main shock formed around 02:47 LT and at the depth of 9 km. Two earthquakes occurred on the western border of Iran are considered. The Gilangharb (GH) earthquake (34.15 N, 45.65 E) occurred on 2019-1-6 at 17:12 LT with 5.9 M, and the Ezgeleh (EZ) earthquake (34.87N, 45.76 E) on 2019-5-11 at 14:58 LT with 5.1 M are studied in this work. Figure 1 shows the location of the 4 mentioned EQs and their relative distance to the LF signal propagation path. The Iranian Seismological Center has determined the focal depths of 11, 16 and 8 for GH, KE, and EZ earthquakes, respectively. These earthquakes occurred in the NW Zagros Fold-Thrust Belt (ZF-TB) where the NW–SE-striking Zagros Mountains belt formed due to the continental collision between the Arabian and Eurasian plates (Alavi, 2007; Vergés et al., 2011). The Zagros Mountains are one of the most rapidly-deforming fold and thrust belts in the world, accommodating almost 50% of the present-day shortening between Arabia and Eurasia (Vernant et al., 2004). This part of the Zagros belt hosts moderate seismicity, (M = 5–6) with depths ranging from 5 to 20 km, however an unusually large earthquake Mw 7.3 on November 12, 2017 hit the region. A pre-seismic anomaly from satellite observations as earthquake-precursor has been reported for this earthquake (Wu et al., 2018; Akhoondzadeh et al., 2019). Local network data demonstrate that microseismicity in ZFTB occurs within the basement, reaching depths of ~20 km and centroid depths of larger (Mw > 5) earthquakes are mostly ~4–14 km, with rare events up to ~20 km (Nissen et al., 2011). The mechanism solutions representing the oblique-thrusts faulting at mid-crustal depth on low angle dipping. Therefore, most earthquakes that occur in Iran plateau are shallow and are located less than 20 km. These earthquakes provide an opportunity to improve our understanding of the region and the associated seismic hazard.

The monthly behavior and evolution of the LF signal presented in the previous section will be implemented here to characterize the deviation of the radio signal from its normal pattern due to earthquake activities. The first earthquake studied in this paper occurred on 2019/11/07 near East Azerbaijan province in the north-west of Iran (37.71 N, 47.52 E). The LF data from two transmitters in Turkey is analyzed within +/-15 days of the event. The 162 kHz radio signal received at the Tehran (TEH) station is shown in Figure 6. According to the diurnal variation of 162 kHz radio signal within +/- 15 days of the EQ event on 2019/11/7, the minimum amplitude of the signal is approximately 10 dB for days before and after the EQ. For days close to the EQ, the minimum amplitude drops a few dB. Another noticeable characteristic observed in the data is the variation of sunrise and sunset termination time for days before and after the EQ.

To perform a detailed analysis of the LF radio signal, the zoomed-in sunrise termination time (left panels) and sunset termination time associated with 180 kHz radio signal within +/- 15 days of the EQ

event on 2019/11/7 are shown in Figure 7. The two propagation paths close to the epicenter of the EQ show a similar trend in the signal characteristics. Specifically, the sunrise termination time shifts randomly about 24 and 18 minutes, three and two weeks before the EQ. Within 5 days before and after the EQ, the sunrise termination time shows less than 6 minutes variation. Two and three weeks after the event the termination time alters 24 and 36 minutes daily within a 5 day time period. Similar anomalous variation of the LF signal at 162 and 180 kHz is also observed for results of sunset set termination time. According to Figures 4 and 5, sunset termination time varies 12, 48, 10, ~ 5, ~24 and 60 minutes, for -15, -10, -5, 0, 5, 10 and 15 days with the respect to the EQ day.
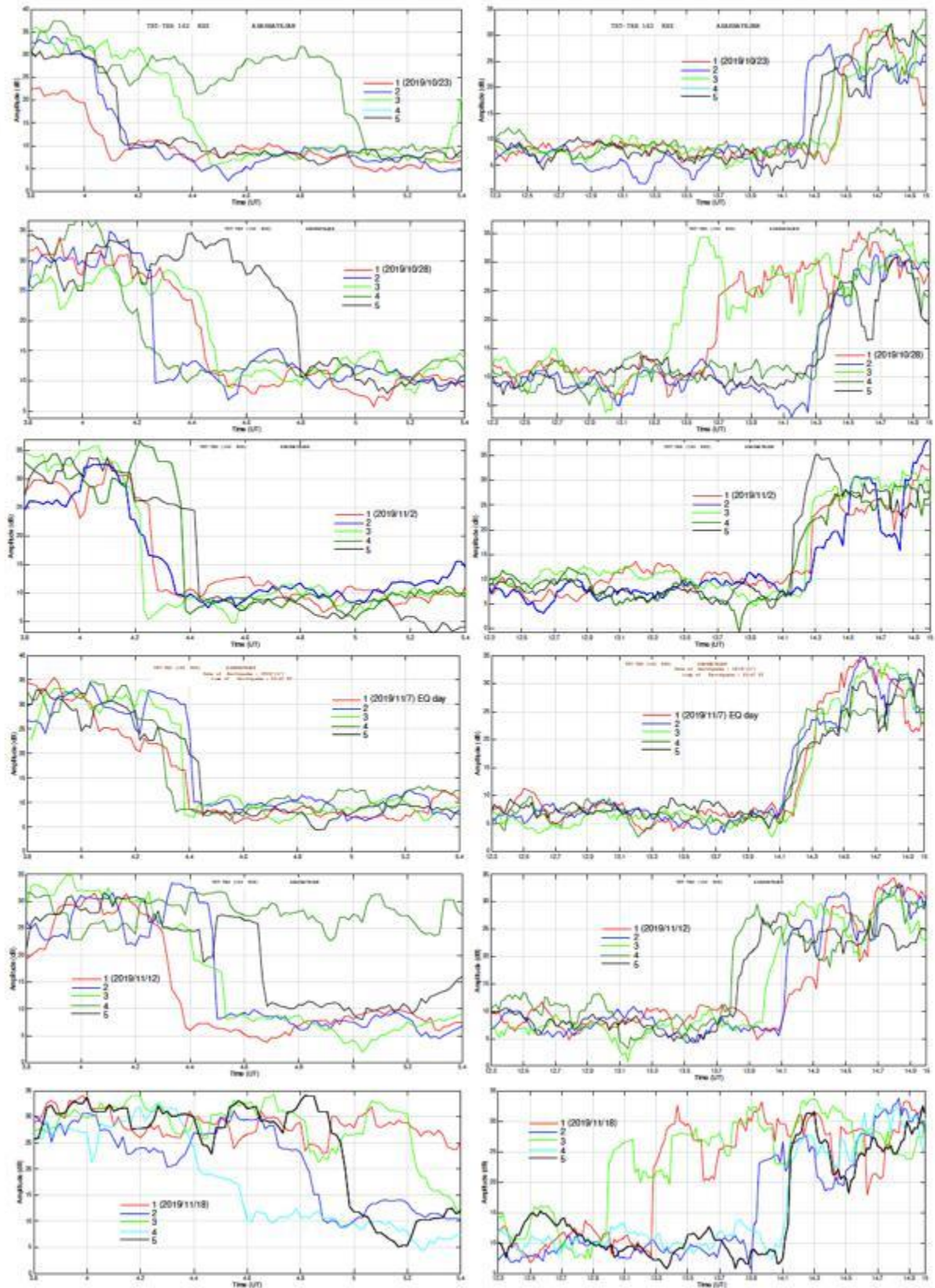
Figure 6. The zoomed in sunrise termination time (left panels) and sunset termination time associated with 162 kHz radio signal within _+/-15 days of the EQ event on 2019/11/7.
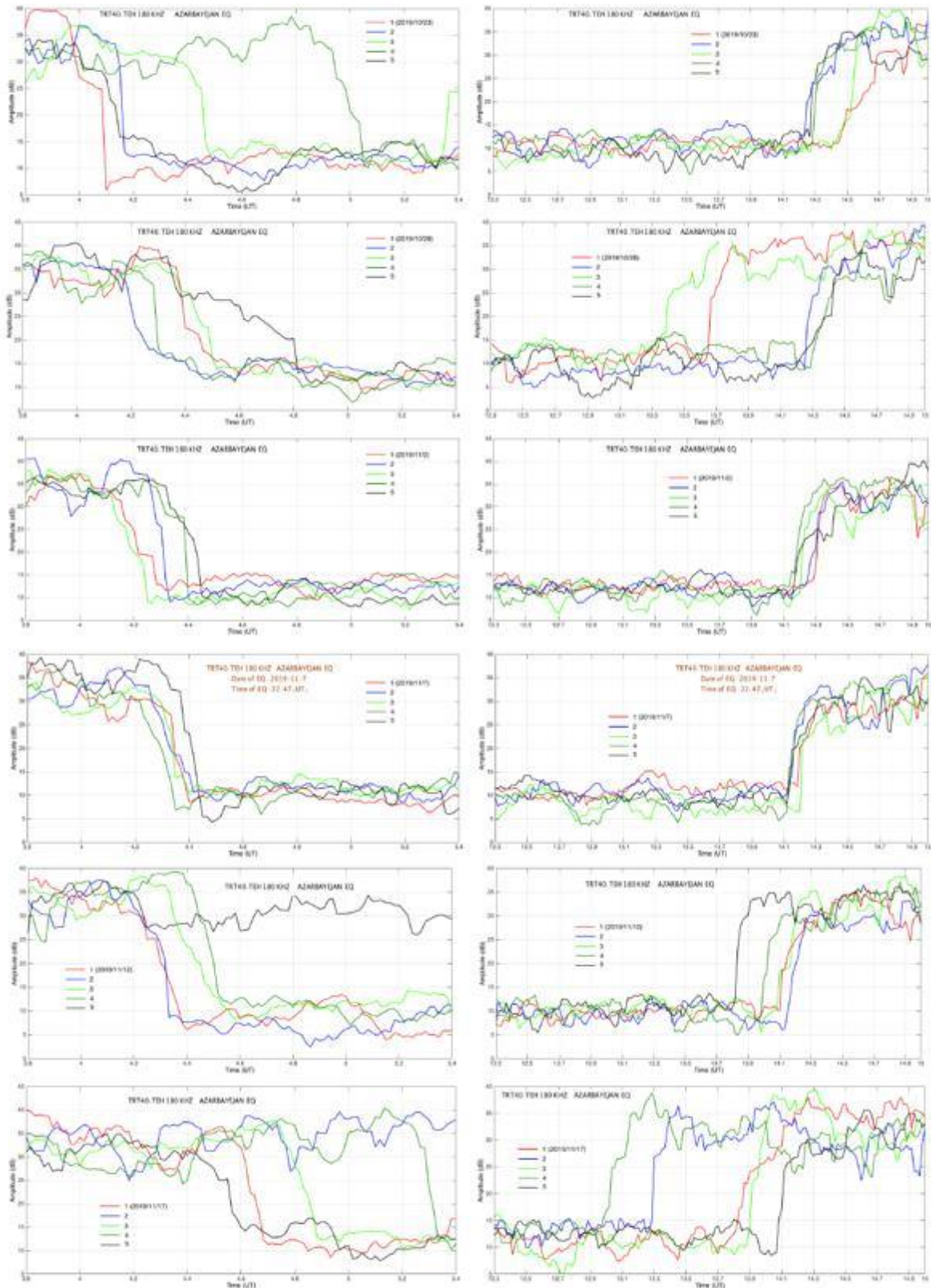
Figure 7. The zoomed in sunrise termination time (left panels) and sunset termination time associated with 180 kHz radio signal within +/- 15 days of the EQ event on 2019/11/7.

Figure 8 represents the morning termination time (T_M) and the evening termination time (T_E). The main purpose of this figure is to determine the days with abnormal daytime (T_M-T_E) in the LF data.

The obtained daytime variation obtained using the LF data are studied associated with the East Azerbaijan EQ along with 3 EQs in the western part of Iran that occurred during 2019. The various distance of the selected EQs with respective to the LF signal propagation path is considered to characterize the signal sensitivity to the possible ionospheric irregularities produced by the LAIC process. According to Figure 8a, at least between 3 to 4 days with a shorter period than the normal daytime are distinguished within -7 to -14 days before the East Azerbaijan EQ. A few days with irregular daytime are also observed between +7 to +14 days after the mainshock. The smooth trend of T_E and T_M curved shown with the blue line is pronounced in comparison with the EQs that occurred at a larger distance relative to the LF signal path (Figure 8b, c, and d). A close comparison of the Figures shows that the number of days with anomalous daytime is greatly dependent on the distance to the LF path. As the distance to the signal propagation path increases from Ezgeleh EQ to Gilangharb EQ, and Kermanshah EQ, the extended period before the EQ day reduces from -11 to -9, and -7, respectively. Therefore, the shorter distance to the LF propagation path can impact the possibility of EQ prediction as well as the number of days before the event that anomalies start to appear. Moreover, the fuzzy behavior of T_E and T_M associated with the 3 EQs located further apart from the signal path emphasized the importance of proximity to the propagation path for a more accurate prediction.
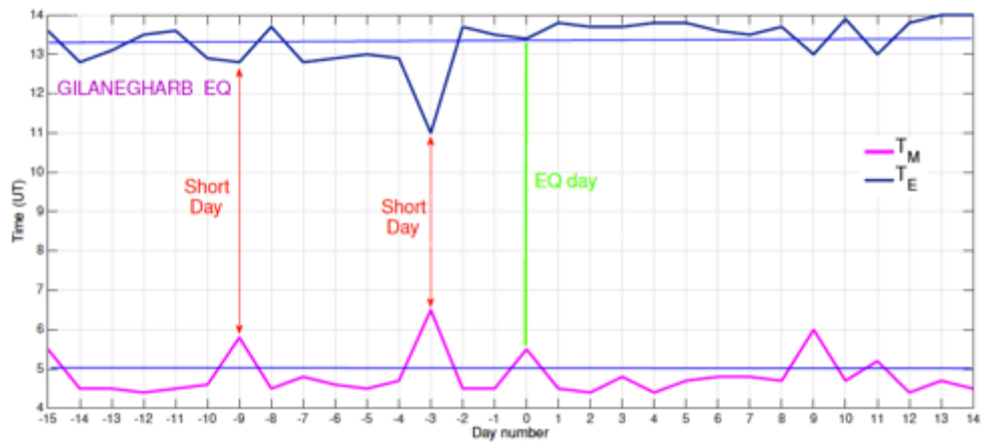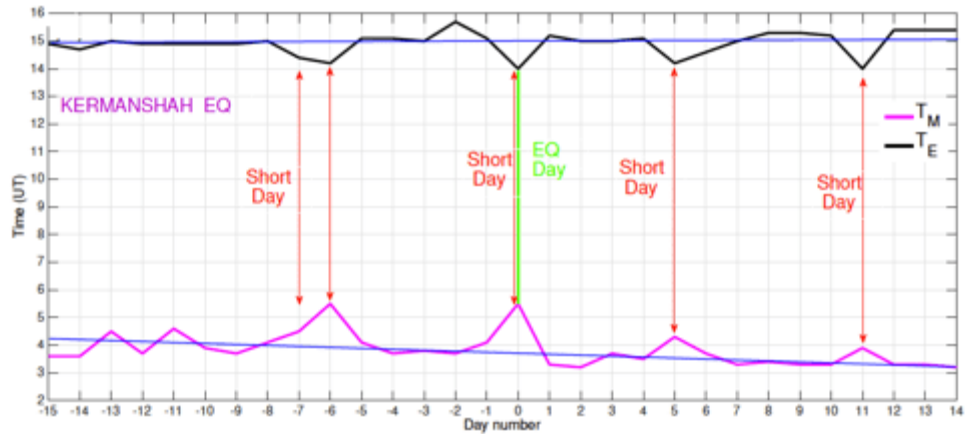
(a)
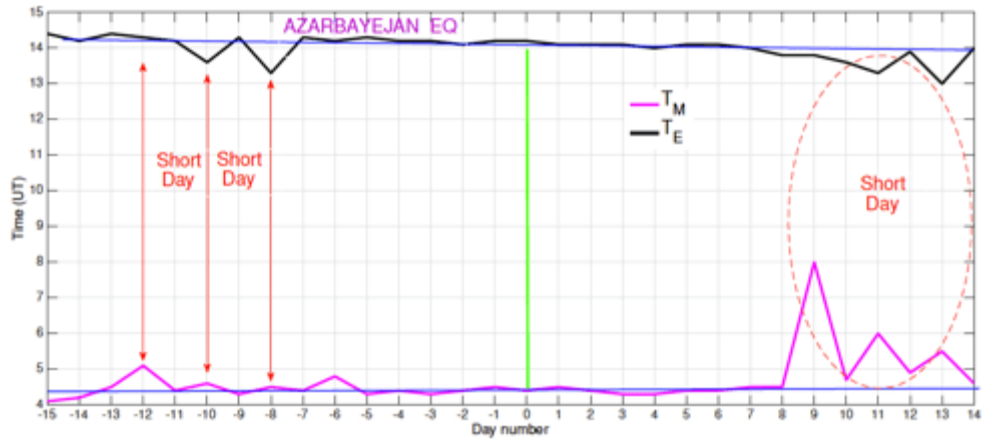
(b)
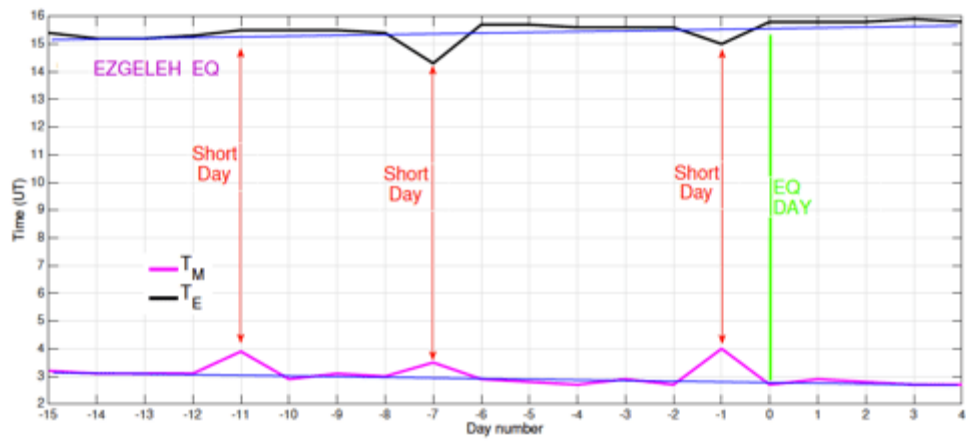
(c)

(d)

Figure 8. The morning termination time (TM) shown in red as well as the evening termination time (TE) shown in blue for a) East Azerbaijan EQ (2019-5-11), b) Ezgeleh EQ (2019-5-11), c) Gilangharb EQ (2019-1-6), and d) Kermanshah EQ (2019-4-1). The anomalous signal variations including signature of shortened day are depicted.

6. Summary and conclusion

The LF radio sounding over the Iran area is studied in detail in this paper for the purpose of ionospheric remote sensing, improve IRI prediction, and earthquake prediction. The paper studies two separate concepts as indicated in the title. Ionospheric remote sensing concept mainly used the termination time associated with the morning and afternoon in the LF data. In fact, the steepness of increase and decay in the amplitude curve is used. The rate of increase is compared with the IRI data to validate the LF data in the first step. Then, it has been proposed that shape including the rate of LF signal amplitude in time can be compared with the rate of electron density and as a result a machine learning approach can be developed to estimate the best fit of electron density profile along the signal propagation path. Such technique using several receiving stations which is currently being installed over Iran could result in regional improvement to the IRI model.

As mentioned, the main features of the received signal such as morning and evening termination time, seasonal variation of the timing and amplitude of the LF signal are investigated. The behavior of the sounded LF signal (averaged over one month period to eliminate temporal ionospheric variation) over long distances by reflecting from the ionosphere is validated through comparison with electron density variation along the propagation path. The comparison of the observed LF data and the averaged electron density along the transmission path obtained through the IRI show a good agreement. Specifically, the IRI model predicts the sunrise and sunset termination time with reasonable accuracy. There is a slight difference in the amplitude of the accumulated density and suppression level of the LF signal. This could be justified by a slight difference in the selected path of propagation, a small number of points used in the study, or a general limitation of the IRI model in the ionospheric density prediction. The electron density altitude profile in the range of 80-140 km is studied in order to validate the diurnal time variation of the sounded LF signals. The amplitude of the observed signal also shows a good correlation with maximum electron density predicted by the IRI model, which denotes an increase in the number of reflection paths. The fall and rise time of the radio signal over the straight path in the longitudinal direction shows a good agreement with the rise and fall period of electron density predicted by the IRI model that can be implemented for ionospheric remote sensing. Moreover, data assimilation technique can be developed to improve IRI model prediction using network observation for different combinations of transmitters and receivers.

The LF data recorded from two transmitters in Turkey at 162 kHz and 180 kHz are examined within +/- 15 days of an earthquake which was occurred in the northwest of Iran. The East Azerbaijan earthquake was in the west-north of Iran (37.71 N, 47.52 E) at the depth of 9 km. The detailed analysis of the two LF signal revealed that between 15 days to 5 days before the EQ, the sunrise and sunset termination time show a strong deviation and a time shift of the order of 24 and 48 minutes, respectively. The maximum anomalous change in the sunset and sunrise termination time was observed 12 and 7 days prior to the EQ, respectively. The termination time shows a minimum shift of fewer than 5 minutes within +/- 5 days. This could be attributed to the propagation of radio signal through perturbed ionosphere above the epicenter that could change the ionospheric hobs. The radio signal propagated through the disturbed ionosphere will experience additional reflection in the earth-ionosphere waveguide. This manifest itself as a delay especially during the termination time that the ionosphere experience the maximum electron density variation. The analysis presented in this paper revealed that the number of days with anomalous daytime is greatly dependent on the distance to the LF path. It has been shown that as the distance to the signal propagation path increases from Ezgeleh EQ to Gilangharb EQ, and Kermanshah EQ, the extended period before the EQ day reduces from -11 to -9, and -7, respectively. As a result, the shorter distance to the LF propagation path can impact the

possibility of EQ prediction as well as the number of days before the event that anomalies start to appear. This is consistent with the previous finding associated with pre-seismic anomalies on the sounded VLF radio signal (Mahmoudian et al., 2022).

Using the network observation for different combinations of transmitters and receivers would result in a better locating and prediction of the EQ activity. Such a goal is being pursued through 8 planned receiving stations around Iran as a result of the present study. More frequency sounding close to the EQ epicenter could lead to characterization of the ionospheric perturbation.

References

Akhoondzadeh, M., De Santis, A., Marchetti, D., Piscini, A., & Jin, S. (2019). Anomalous seismo-LAI variations potentially associated with the 2017 Mw = 7.3 Sarpol-e Zahab (Iran) earthquake from Swarm satellites, GPS-TEC and climatological data. Adv. Space Res, 64, 143-158, doi:10.1016/j.asr.2019.03.020

Alavi, M. (2007). Structures of the Zagros fold-thrust belt in Iran. Am. J. Sci., 307, 1064–1095, https://doi.org/10.2475/09.2007.02.

Asai, S., Yamamoto, S., Kasahara, Y., Hobara, Y., Inaba, T., & Hayakawa M. (2011). Measurement of Doppler shifts of short-distance subionospheric LF transmitter signals and seismic effects. J. Geophys. Res., 116, A02311,doi:10.1029/2010JA016055.

Bilitza, D., Altadill, D., Truhlik, V., Shubin, V., Galkin, I., Reinisch, B., & Huang X. (2017). International Reference Ionosphere 2016: From ionospheric climate to real-time weather predictions. Space Weather, 15, 418-429, doi:10.1002/2016SW001593.

Bilitza, D. (2018). IRI the International Standard for the Ionosphere. Adv. Radio Sci., 16, 1-11, https://doi.org/10.5194/ars-16-1-2018.

Cohen, M. B., Gross, N. C., Higginson-Rollins, M. A., Marshall, R. A., Gołkowski, M., Liles, W., et al. (2018). The lower ionospheric VLF/LF response to the 2017 Great American Solar Eclipse observed across the continent. Geophysical Research Letters, 45, 3348–3355. https://doi.org/10.1002/2018GL077351

Cohen, M. B., Inan U. S., & Paschal, E. W. (2010). Sensitive Broadband ELF/VLF Radio Reception With the AWESOME Instrument. in IEEE Transactions on Geoscience and Remote Sensing, 48, 1, 3-17, doi: 10.1109/TGRS.2009.2028334.

Conti, L., Picozza , P., & Sotgiu, A. (2021). A Critical Review of Ground Based Observations of Earthquake Precursors. Front. Earth Sci. 9:676766. doi: 10.3389/feart.2021.676766

Ghosh, S., Chowdhury, S., Kundu, S., Sasmal, S., Politis, D.Z., Potirakis, S.M., Hayakawa, M., Chakraborty, S., Chakrabarti, S.K. (2022). Unusual Surface Latent Heat Flux Variations and Their Critical Dynamics Revealed before Strong Earthquakes. Entropy., 24, 23. https://doi.org/10.3390/e24010023.

Gross, N. C., & Cohen, M. B. (2020). VLF remote sensing of the D region ionosphere using neural networks. Journal of Geophysical Research: Space Physics, 125, e2019JA027135. https://doi.org/10.1029/2019JA027135

Hayakawa, M., Kasahara, Y., Nakamura, T., Muto, F., Horie, T., Maekawa, S., Hobara, Y., Rozhnoi, A. A, Solovieva, M., & Molchanov, O. A. (2010a). A statistical study on the correlation between lower ionospheric perturbations as seen by subionospheric VLF/LF propagation and earthquakes. J. Geophys. Res., 115, A09305, doi:10.1029/2009JA015143.

Hayakawa, M., Kasahara, Y., Nakamura, T., Hobara, Y., Rozhnoi, A., Solovieva, M., & Molchanov, O. A. (2010b). On the correlation between ionospheric perturbations as detected by subionospheric VLF/LF signals and earthquakes as characterized by seismic intensity. J. Atmos. Sol. Terr. Phys., 72, 982–987, doi:10.1016/j.jastp.2010.05.009.

Hayakawa, M., Horie, T., Muto, F., Kasahara, Y., Ohta, K., Liu, J.Y., & Hobara, Y. (2010c). Subionospheric VLF/LF probing of ionospheric perturbations associated with earthquakes: A possibility of earthquake prediction. SICE J. Control, Meas., and Syst. Integration, 3(1), 10–14.

Hayakawa, M. (2016). Earthquake Prediction with Radio Techniques. Singapore: Wiley.

Hayakawa, M., Izutsu, J., Schekotov, A., Yang, S.-S., Solovieva, M., Budilova, E. Lithosphere–Atmosphere–Ionosphere Coupling Effects Based on Multiparameter Precursor Observations for February–March 2021 Earthquakes (M~7) in the Offshore of Tohoku Area of Japan. Geosciences 2021, 11, 481.

Kumar, A., Kumar, S., Hayakawa, M., & Menk, F., (2013). Subionospheric VLF perturbations observed at low latitude associated with earthquake from Indonesia region. Journal of Atmospheric and Solar-Terrestrial Physics, 102, 71-80, https://doi.org/10.1016/j.jastp.2013.04.011.

Kumar, S., Kumar, S., Kumar, & A., (2022). Earthquakes associated subionospheric VLF anomalies recorded at two low latitude stations in the South Pacific region. Journal of Atmospheric and Solar-Terrestrial Physics, 229, https://doi.org/10.1016/j.jastp.2022.105834.

Kundu, S., Chowdhury, S., Gosh, S., Sasmal, S., Politis, D., Potirakis, S. M., Yang, S.S., Chakrabarti, S.K., Hayakawa, M. (2022). Seismogenic anomalies in Atmospheric Gravity Waves observed by SABER/ TIMED satellite during large earthquakes. J. Sens. 2022, 3201104.

Mahmoudian, A., Mohebalhojeh, A. R., & Safari, M. (2021). Investigation of VLF radio sounding for studying semi-diurnal tide and gravity waves. Geophysical Research Letters, 48, e2021GL092949. https://doi.org/10.1029/2021GL092949

Mahmoudian, A., Safari, M. & Rezapour, M. (2022). Earthquake prediction assessment using VLF radio signal sounding and space-based ULF emission observation. Acta Geophys. 70, 1269–1284 https://doi.org/10.1007/s11600-022-00785-9

Molchanov, O. A., Hayakawa, M., Ondoh, T., & Kawai, E. (1998). Precursory effects in the subionospheric VLF signals for the Kobe earthquake. Phys. Earth Planet. In., 105, 239–248.

Molchanov, O., Fedorov, E., Schekotov, A., Gordeev, E., Chebrov, V., Surkov, V., Rozhnoi, A., Andreevsky, S., Iudin, D., Yunga, S., et al. (2004). Lithosphere-atmosphere-ionosphere coupling as governing mechanism for preseismic short-term events in atmosphere and ionosphere. Nat. Hazards Earth Syst. Sci., 4, 757–767.

Nissen, E., Tatar, M., Jackson, J.A. & Allen, M.B. (2011). New views on earthquake faulting in the Zagros fold-and-thrust belt of Iran. Geophysical Journal International, 186, 928–944, doi: 10.1111/j.1365-246X.2011.5119.x.

Ouzounov, D., Hattori, K., Taylor, P., Pulinets, P. S. (2018). Pre-Earthquake Processes: A Multidisciplinary Approach to Earthquake Prediction Studies. Wiley, ISBN:9781119156932, 1119156939

Picozza, P., Conti, L., & Sotgiu, A. (2021). Looking for Earthquake Precursors From Space: A Critical Review. Front. Earth Sci. 9:676775. doi: 10.3389/feart.2021.676775

Pulinets S., & Boyarchuk, K. (2005). Ionospheric Precursors of Earthquakes. Springer.

Pulinets, S., & Ouzounov, D. (2011). Lithosphere-atmosphere-ionosphere coupling (LAIC) model—A unified concept for earthquake precursor validation. J. Asian Earth Sci., 41, 371–382, doi:10.1016/j.jseaes.2010.03.005.

Rawer, K., Bilitza, D., & Ramakrishnan, S. (1978). Goals and Status of the International Reference Ionosphere. Rev. Geophys., 16, 177-181.

Richardson, D. K., & Cohen, M. B. (2021). Seasonal variation of the D-region ionosphere: Very low frequency (VLF) and machine learning models. Journal of Geophysical Research: Space Physics, 126, e2021JA029689. https://doi.org/10.1029/2021JA029689

Sorokin, V.V., Chmyrev, V., Hayakawa, M. (2015). Electrodynamic Coupling of Lithosphere-Atmosphere-Ionosphere of the Earth, NOVA Science Pub. Inc.: New York, NY, USA, 355p

Vergés, J., Saura, E., Casciello, E., Fernàndez, M., Villaseñor, A., Jiménez-Munt, I. & García-Castellanos, D. (2011). Crustal-scale cross-sections across the NW Zagros belt: implications for the Arabian margin reconstruction. Geol. Mag., 148, 739–761, https://doi.org/10.1017/S0016756811000331.

Vernant, P., Nilforoushan, F., Hatzfeld, D., Abbassi, M.R., Vigny, C., Masson, F., Nankali, H., Martinod, J., Ashtiani, A., Bayer, R., Tavakoli, F. & Chéry, J. (2004). Present-day crustal deformation and plate kinematics in the Middle East constrained by GPS measurements in Iran and northern Oman. Geophys. J. Int., 157, 381–398, https://doi.org/10.1111/gji.2004.157.issue-1.

Wu, L., Zhou, Y., Miao, Z., & Qin, K. (2018). Anomaly Identification and Validation for Winter 2017 Iraq and Iran Earthquakes, EGU2018-5800, 2018 EGU General Assembly.

Yang, S.-S., Asano, T., Hayakawa, M. (2019). Abnormal gravity wave activity in the stratosphere prior to the 2016 Kumamoto earthquakes. Journal of Geophysical Research: Space Physics., 124, 1410–1425. https://doi.org/10.1029/2018JA026002.

Yang, Sh., Hayakawa, M. (2020). Gravity Wave Activity in the Stratosphere before the 2011 Tohoku Earthquake as the Mechanism of Lithosphere-atmosphere-ionosphere Coupling. Entropy., 22, 110. https://doi.org/10.3390/e22010110.